USING IMAGE-BASED REGRESSION TO ACQUIRE FREEHAND 3D ULTRASOUND

R. W. Prager, A. H. Gee,
G. M. Treece, C. J. C. Cash,
and L. H. Berman

CUED/F-INFENG/TR 436

June 2002

University of Cambridge
Department of Engineering
Trumpington Street
Cambridge CB2 1PZ
England

Email: ahg/rwp/gmt11/cjcc2 @eng.cam.ac.uk, lb@radiol.cam.ac.uk

Using Image-based regression to acquire freehand 3D ultrasound

Richard Prager, Andrew Gee, Graham Treece, Charlotte Cash* and Laurence Berman*
University of Cambridge

Department of Engineering
Trumpington Street
Cambridge CB2 1PZ

*Department of Radiology
Addenbrooke's Hospital
Cambridge CB2 2QQ

Abstract

In freehand 3D ultrasound, a position sensor is attached to the probe of a 2D ultrasound machine. The resulting 3D data permits flexible visualisation and more accurate volume measurement than can be achieved using 2D B-scans alone; however the use of the position sensor can be inconvenient for the clinician. The objective is thus to replace the sensor with a technique for estimating the probe trajectory based on the B-scan images themselves. One such technique exists, based on decorrelation algorithms. This report presents an alternative approach based on linear regression of the echo envelope intensity signal. A probabilistic analysis of the speckle characteristics of the ultrasound signal leads to a linear model on which the regression algorithm is based. The gradient parameter of this model is shown to be directly related to probe motion. The viability of the new approach is demonstrated through simulations, and *in vitro* and *in vivo* experiments.

1 Introduction

Figure 1 shows an ultrasound probe with a position sensor attached in order to perform freehand 3D scanning. A computer is used to record the sensor output describing the trajectory of the probe during the scan, together with the sequence of B-scan images produced by the ultrasound machine. The B-scan images are then reassembled in 3D space based on the position information, enabling interactive visualisation of complex structures and accurate volume measurements.

The position sensor records the absolute positions of each of the B-scan images. To replace this with an image-based technique we have to find the local transformation between each pair of B-scans in the sequence, and then combine these transformations to estimate the overall motion of the probe. Cumulative errors leading to drift will be unavoidable in this process.

Provided it is small, the local transformation between a pair of B-scans can be considered in two independent parts: motion in and motion out of the plane of the B-scan. The in-plane motion consists of two translations and a single rotation about an axis orthogonal

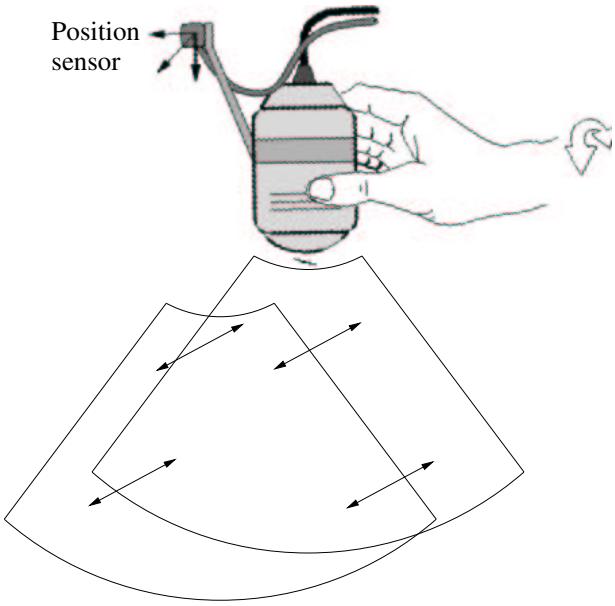

Figure 1: A conventional 2D ultrasound probe with a position sensor attached for freehand 3D scanning. The outlines of two B-scan slices are shown. The arrows between the outlines indicate the motion out of the plane of the scans.

to the average normal to the scans. Estimation of these transformations is essentially a registration problem; the goal is to align corresponding features in neighbouring images.

The out-of-plane motion consists of two rotations and one translation. To estimate these parameters, we have to make use of the fact that the beam from an ultrasound scanner is several millimetres wide, even at the focus. Each pixel in the scan image is sensitive to backscattered echos from a roughly ellipsoidal volume known as the *resolution cell* (see figure 2). The resolution cells of pixels in neighbouring scans will overlap and, as a result, there will be a statistical link between their values. If we can model this link, we can calculate out-of-plane offsets between a pair of B-scans, as shown by the arrows in figure 1, and hence estimate the required translation and rotations.

Previous authors have derived expressions for the autocorrelation function of the speckle signal [2, 13, 1], and developed algorithms for measuring the out-of-plane offsets based on the decorrelation between a pair of images [5, 12]. In this report we present a novel theoretical analysis of the statistics of speckle, leading to a new algorithm for estimating the out-of-plane offsets between neighbouring B-scans. The result is an alternative approach to the acquisition of sensorless freehand 3D ultrasound data.

In section 2, we use Bayes's theorem to develop a model to predict the expected intensity in one scan based on the intensity in a neighbouring scan and the distance between them. The model turns out to be linear, and leads to a simple technique for distance estimation based on linear regression. Simulations are presented in section 3 to confirm the theoretical results. In section 4, we describe our methodology for sensorless freehand scanning, and in section 5 we demonstrate its application in scans of two tissue-mimicking ultrasound

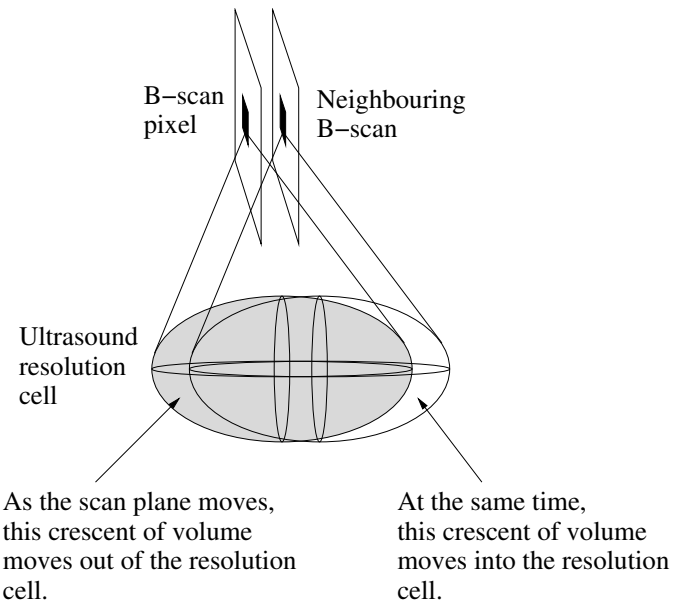

Figure 2: Two pixels on neighbouring B-scans and the ultrasound resolution cells to which they correspond.

phantoms. *In vivo* results for visualisation and volume measurement are presented in section 6. Appendix A presents an extension of the theory to show how it is possible to derive the existing correlation-based distance measurement algorithms using our model.

2 Theory of regression-based distance measurement

In this section we demonstrate how the total back-scattered intensity from a resolution cell in one position affects the value of intensity we expect when the resolution cell is in a neighbouring, overlapping, position. We model the back-scattered signal as the sum of a large number (N) of scatterers that each have a small amplitude r, and random phase θ_i that is uniformly distributed on 0 to 2π. The total back-scattered intensity I is given by:

$$I = x^2 + y^2 \tag{1}$$

$$x = \sum_{i=1}^{N} r\cos(\theta_i) \tag{2}$$

$$y = \sum_{i=1}^{N} r\sin(\theta_i). \tag{3}$$

By the central limit theorem, both x and y will be Gaussian distributed with zero mean and variance $\frac{1}{2}r^2N$. If we have no prior knowledge of neighbouring intensity values, the expected value of I can be expressed in terms of the means (μ_x and μ_y), and variances (σ_x^2

and σ_y^2), of x and y.

$$\begin{aligned}\langle I\rangle &= \int\int_{-\infty}^{+\infty} \frac{x^2+y^2}{2\pi\sigma_x\sigma_y}\exp\left(-\frac{(x-\mu_x)^2}{2\sigma_x^2}-\frac{(y-\mu_y)^2}{2\sigma_y^2}\right)\mathrm{d}x\mathrm{d}y \\ &= \mu_x^2+\mu_y^2+\sigma_x^2+\sigma_y^2 \qquad (4)\\ &= r^2N \qquad (5)\end{aligned}$$

Suppose that we know the value of I when the resolution cell is at position 1 in the body. Call this I_1. We want to know the expected value of I when the resolution cell has been moved a small distance to position 2. We wish to find $\langle I_2\rangle$ as a function of I_1.

As the resolution cell moves from 1 to 2, some scatterers (say q) will leave, to be replaced by an equal number of different scatterers: see figure 2. Consider first just the x component of the scattered signal at position 1, which we will call x_1. This can be thought of as being made up of two elements $x_1 = T + Q$, where Q is Gaussian distributed with variance $\sigma_q^2 = \frac{1}{2}r^2q$, and T is Gaussian distributed with variance $\sigma_t^2 = \frac{1}{2}r^2(N-q)$. Using Bayes's rule

$$\begin{aligned}\mathrm{p}(T|x_1) &= \frac{\mathrm{p}(T)\mathrm{p}(x_1|T)}{\mathrm{p}(x_1)} \\ &= \frac{\exp\left(\frac{-T^2}{2\sigma_t^2}\right)}{\sigma_t\sqrt{2\pi}}\cdot\frac{\exp\left(\frac{-(x_1-T)^2}{2\sigma_q^2}\right)}{\sigma_q\sqrt{2\pi}}\cdot\frac{\sqrt{2\pi(\sigma_t^2+\sigma_q^2)}}{\exp\left(\frac{-x_1^2}{2(\sigma_t^2+\sigma_q^2)}\right)} \qquad (6)\end{aligned}$$

We can thus calculate the expected value of T given x_1.

$$\langle T|x_1\rangle = \int_{-\infty}^{\infty} T\mathrm{p}(T|x_1)dT = \frac{x_1\sigma_t^2}{\sigma_t^2+\sigma_q^2}$$

Similarly the variance of T given x_1 can be found.

$$\left\langle (T|x_1)^2\right\rangle - \langle T|x_1\rangle^2 = \frac{\sigma_t^2\sigma_q^2}{\sigma_t^2+\sigma_q^2}$$

The distribution of $T|x_1$ relates to the volume of the left hand resolution cell in figure 2, once the crescent on its left has been removed. To work out the x contribution to the right hand resolution cell (*i.e.* x_2), we need to add a figure to represent the crescent that is added on the right. This is an independent Gaussian variable with zero mean and variance σ_q^2. Thus

$$\begin{aligned}\langle x_2|x_1\rangle &= \frac{x_1\sigma_t^2}{\sigma_t^2+\sigma_q^2} \\ \left\langle (x_2|x_1)^2\right\rangle - \langle x_2|x_1\rangle^2 &= \frac{\sigma_t^2\sigma_q^2}{\sigma_t^2+\sigma_q^2}+\sigma_q^2 = \frac{\sigma_q^2(2\sigma_t^2+\sigma_q^2)}{\sigma_t^2+\sigma_q^2}\end{aligned}$$

Similar results can be derived for $\langle y_2|y_1\rangle$. We can now use equation (4) to give the expected value of I_2.

$$\begin{aligned}\langle I_2|I_1\rangle &= \mu_x^2+\mu_y^2+\sigma_x^2+\sigma_y^2 \\ &= x_1^2\left(\frac{\sigma_t^2}{\sigma_t^2+\sigma_q^2}\right)^2+y_1^2\left(\frac{\sigma_t^2}{\sigma_t^2+\sigma_q^2}\right)^2+2\frac{\sigma_q^2(2\sigma_t^2+\sigma_q^2)}{\sigma_t^2+\sigma_q^2} \\ &= I_1\left(\frac{\sigma_t^2}{\sigma_t^2+\sigma_q^2}\right)^2+\frac{2\sigma_q^2(2\sigma_t^2+\sigma_q^2)}{\sigma_t^2+\sigma_q^2} \end{aligned} \tag{7}$$

We know that the overall expected intensity of the signal $\langle I\rangle = 2(\sigma_t^2+\sigma_q^2)$. The intensity of the q scatterers that move either in or out of the resolution cell equals $2\sigma_q^2$, call this $\langle i\rangle$. Equation (7) can thus be written

$$\langle I_2|I_1\rangle = I_1\left(1-\frac{\langle i\rangle}{\langle I\rangle}\right)^2+\langle i\rangle\left(2-\frac{\langle i\rangle}{\langle I\rangle}\right) \tag{8}$$

Let

$$b=\left(1-\frac{\langle i\rangle}{\langle I\rangle}\right)^2 \tag{9}$$

and

$$a=\langle i\rangle\left(2-\frac{\langle i\rangle}{\langle I\rangle}\right) \quad .$$

Given samples of ultrasound intensity data recorded at position 1 and position 2, b can be found from equation (8) by computing a regression of I_2 as a function of I_1. This involves finding the least mean squared error solution of the following equation:

$$\begin{pmatrix} I_{2,1}\\ I_{2,2}\\ I_{2,3}\\ I_{2,4}\\ \vdots\\ I_{2,n}\end{pmatrix} = \begin{pmatrix} I_{1,1} & 1\\ I_{1,2} & 1\\ I_{1,3} & 1\\ I_{1,4} & 1\\ \vdots & \vdots\\ I_{1,n} & 1\end{pmatrix}\begin{pmatrix} b\\ a\end{pmatrix} \tag{10}$$

$$\boldsymbol{y} = M\boldsymbol{x}$$

One way of solving this is to compute $\hat{\boldsymbol{x}} = \left(M^TM\right)^{-1}M^T\boldsymbol{y}$. This only involves inverting a 2×2 matrix and so is not difficult.

Note that it is equally valid to compute a regression of I_1 given I_2 as it is to compute a regression of I_2 given I_1. To make full use of any available data, we thus include both I_1 and I_2 in both $\boldsymbol{y}$ and M.

Having established a link between the intensity data and b, and using equation (9) to connect b with $\langle i\rangle$, we now need to derive a relationship between $\langle i\rangle$ and the distance between position 1 and position 2. This depends on the shape of the ultrasound resolution cell.

2.1 Rectangular resolution cell

For a rectangular resolution cell, moved so that q scatterers leave and are replaced,

$$\begin{aligned} \langle I \rangle &= Nr^2 \\ \langle i \rangle &= qr^2 \\ \Rightarrow \langle I_2 | I_1 \rangle &= I_1 \left(1 - \frac{q}{N}\right)^2 + qr^2 \left(2 - \frac{q}{N}\right) \end{aligned} \tag{11}$$

If the movement is in a direction parallel to an edge of the resolution cell, we can estimate q/N as the fraction of the width of the cell that the ultrasound probe has moved. If the width of the cell is w and the distance moved is δ then

$$\begin{aligned} b &= \left(1 - \frac{\delta}{w}\right)^2 \\ \Rightarrow \delta &= w\left(1 - \sqrt{b}\right) \end{aligned}$$

2.2 Gaussian resolution cell

A two dimensional calculation is sufficient to produce a result that is equally valid for three dimensional resolution cells. Consider two Gaussian resolution cells of amplitude A offset by a distance δ. The standard deviation of the width of the cells in the direction of the offset is σ_u, the cell width in the orthogonal direction is σ_v.

$$\begin{aligned} f(u,v) &= \frac{A \exp\left(-\frac{u^2}{2\sigma_u^2} - \frac{v^2}{2\sigma_v^2}\right)}{2\pi\sigma_u\sigma_v} \\ g(u,v) &= \frac{A \exp\left(-\frac{(u-\delta)^2}{2\sigma_u^2} - \frac{v^2}{2\sigma_v^2}\right)}{2\pi\sigma_u\sigma_v} \end{aligned}$$

If the scattering intensity is k^2 then

$$\begin{aligned} \langle I \rangle &= k^2 \iint_{-\infty}^{+\infty} \left(f(u,v)\right)^2 \mathrm{d}u\mathrm{d}v = \frac{k^2 A^2}{4\pi\sigma_u\sigma_v} \\ \langle i \rangle &= \frac{1}{2}k^2 \iint_{-\infty}^{+\infty} \left(g(u,v) - f(u,v)\right)^2 \mathrm{d}u\mathrm{d}v \qquad (12) \\ &= k^2 A^2 \left[\frac{1 - \exp\left(\frac{-\delta^2}{4\sigma_u^2}\right)}{4\pi\sigma_u\sigma_v}\right] \\ \Rightarrow \langle I_2 | I_1 \rangle &= I_1 \exp\left(\frac{-\delta^2}{2\sigma_u^2}\right) + \langle I \rangle \left[1 - \mathrm{e}^{\left(\frac{-\delta^2}{2\sigma_u^2}\right)}\right] \qquad (13) \end{aligned}$$

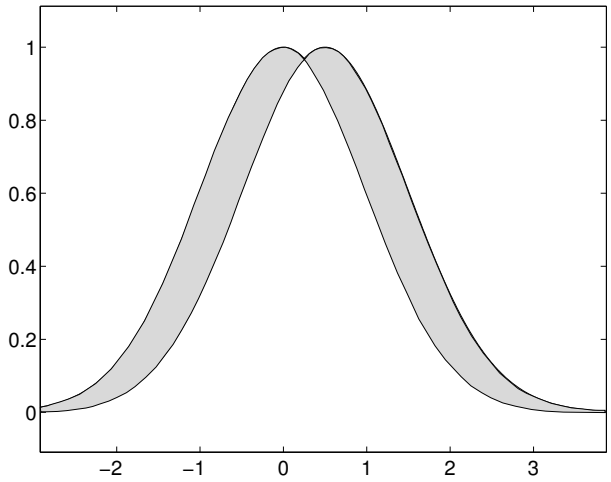

Figure 3: Two overlapping Gaussians. The total shaded area is an illustration of the double integral in equation (12).

The double integral in equation (12) gives the total change in intensity due to scatterers moving in and out of the resolution cell. Figure 3 gives a one-dimensional illustration of this. The integral corresponds to *both* the shaded segments in the figure. To get $\langle i \rangle$, which is the expected intensity change in just one direction, *i.e.* just one shaded region in figure 3, we need to include the $\frac{1}{2}$ as shown. Using the result of the regression analysis:

$$\begin{aligned} b &= \exp\left(\frac{-\delta^2}{2\sigma_u^2}\right) \\ \Rightarrow \delta &= \sqrt{-2\sigma_u^2 \ln(b)} \end{aligned} \tag{14}$$

We can thus use equation (10) to calculate b from the ultrasound image intensity and, provided there is no in-plane misalignment between the B-scans, we can use equation (14) to estimate the separation of the resolution cells using b and σ_u, the width of the resolution cells in the elevational direction.

3 Simulations

Two simulations were performed using intensity data generated using equations (1)–(3). The first simulation was with a rectangular resolution cell of width 91 pixels and the second was with a Gaussian resolution cell with a standard deviation of 10 pixels. In both cases, samples of 5000 pixels were taken as the cells were gradually moved apart. Figure 4 shows a comparison of the real distance the cells have been moved and the distance predicted from the regression coefficients using the theory.

In the simulation with the Gaussian resolution cell, the error has a maximum of 0.08 pixels and an RMS value of 0.06 pixels. In the simulation with the rectangular resolution

cell, the absolute error remains in the range $+0.13$ to -0.43 pixels, with an RMS value of 0.21 pixels. In the rectangular case, $\langle i \rangle$ is made up of 91 components, whereas in the Gaussian case, many hundreds of components are involved. The central limit theorem assumption implicit in equation (6) is therefore more valid in the Gaussian case, and this leads to the lower errors.

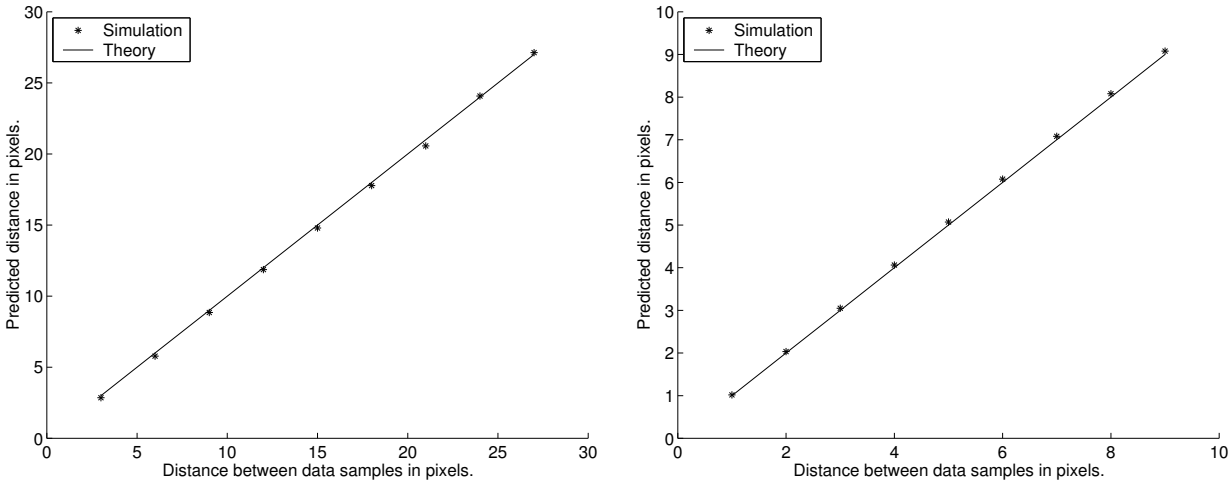

(a) Rectangular resolution cell

(b) Gaussian resolution cell

Figure 4: Simulation results to assess distance measurements based on the regression algorithm.

4 Methodology for 3D sensorless freehand scanning

We list here the steps in our implementation of the algorithm for the reconstruction of freehand 3D ultrasound from the B-scan image sequence alone. This will be used in future sections as a basis for *in vitro* and *in vivo* experiments.

1. The resolution cell of the ultrasound scanner is assumed to be Gaussian in shape. To estimate its dimensions, a small part of the object (not overlapping with the part that is the subject of the main scan) is scanned with a position sensor attached to the ultrasound probe. The distances between various points on the B-scans, as measured by the position sensor, are used together with regression calculations to derive estimates of the elevational width of the ultrasound resolution cell at the top, middle and bottom of the scan image.

2. The object of interest is scanned without a position sensor.

3. In-plane transformations between the B-scan images are estimated using a correlation algorithm as described in [11], with one addition. Treece et al. extract only the two in-plane translations, on the assumption that there is no in-plane rotation. To extend this work to extract any in-plane rotation that may be present, we divide each B-scan into 20 horizontal strips and correlate them individually with the corresponding strips in a neighbouring scan to determine the point of best match. A random sample consensus (RANSAC) algorithm is applied to the 20 measured offsets, and a least mean squares estimate of the horizontal translation and in-plane rotation is calculated using measurements from the strips that are accepted by the RANSAC algorithm [3].

4. The B-scan images are decompressed as described in [8, 9] to extract an approximate intensity signal.

5. A number of patches are defined, covering the majority of the image. For rectilinear probes, nine patches are used in a regular grid. For curvilinear probes, eight patches are used, arranged symmetrically about the centreline of the image.

6. The regression algorithm, as described in section 2, is applied to each pair of aligned patches (taking into account the in-plane transformation that has already been found). The resolution cell dimensions are combined with the regression results using equation (14) to produce a set of offset values referred to the centres of each of the patches.

7. A RANSAC algorithm is applied to the offset values to eliminate incorrect measurements resulting from regions of the ultrasound image that do not contain fully developed speckle. A best-fit plane is computed using the remaining offsets to estimate the overall out-of-plane transformation between the pair of B-scans.

8. The positions of all the slices are computed by assuming that the scan motion is consistently in the same direction. To reduce cumulative errors from persistence in the image from the ultrasound machine, the odd numbered slices are first reconstructed as a complete sequence, ignoring the even numbered slices. Each even numbered slice is then located with reference to the slice immediately before it.

5 Ultrasound data of phantoms

In this section we present two experiments to evaluate the distance measurement algorithm using ultrasound scans of tissue-mimicking phantoms. In the first experiment, the ultrasound probe is mounted in a rigid mechanical assembly to enable the acquisition of slices with accurate known spacing with which the regression-based measurements can be compared. In the second experiment, the methodology described in section 4 is used to scan a phantom containing spheres and the consistency of the reconstruction of the sphere locations is evaluated.

The first experiment involved scans of a uniform tissue-mimicking phantom manufactured by the Department of Medical Physics at Edinburgh Royal Infirmary, UK. Two sets of data were recorded using a Diasus ultrasound machine[1] on different occasions, using different time-gain compensation settings. In both cases the machine was set to record images of maximum depth 81 mm with a single focus just below 41 mm. We do not have direct access to the envelope intensity signal internal to the ultrasound machine. This was therefore estimated using decompression techniques described in [8, 9].

The probe was mounted on a mechanical assembly such that it could be translated slowly in the out-of-plane direction by means of a screw thread. The distances moved were measured using dial-gauges. In the first recording, 50 slices were recorded $\frac{1}{1000}$ of an inch apart. In the second recording, 100 slices were recorded 0.02 mm apart.

After decompression, a patch of 147×119 pixels was extracted from the middle of each ultrasound image, centred at the focus. These were analysed using the regression algorithm and the results are shown as scatter plots in figure 5. The graph in figure 5(a) is consistent with a resolution cell width of standard deviation 0.46 mm, and for figure 5(b), 0.42 mm. Because of the uniform distances between the B-scans in this experiment, the points in both scatter plots are clustered in vertical strips. The lengths of the strips show the maximum variation in the output of the regression algorithm for a given scan separation. For distance measurement, we are more interested in the maximum distance error for a given regression algorithm output. This can be estimated from the horizontal width of the band of strips.

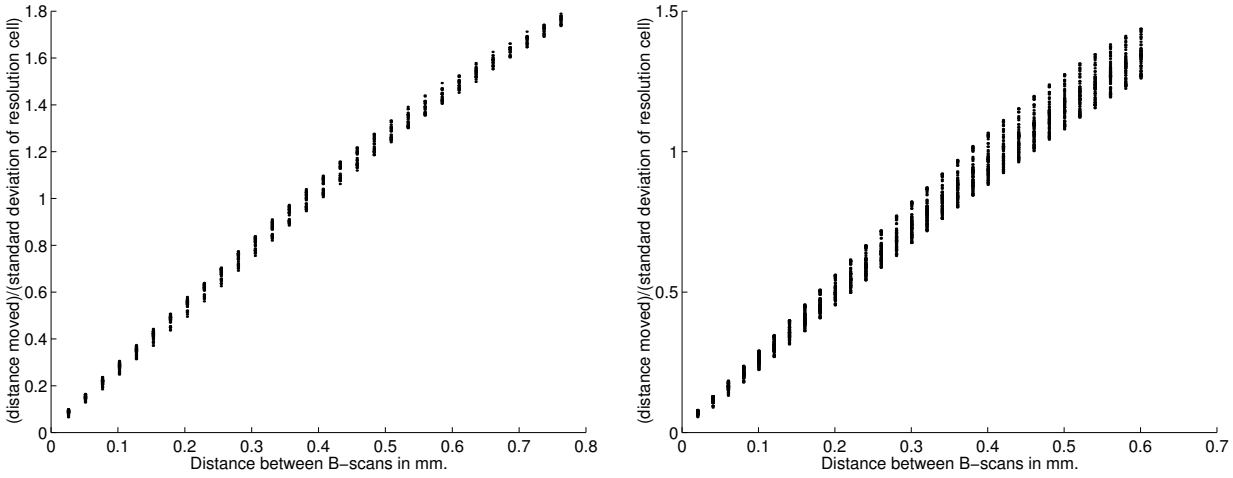

(a) Using 50 slices 1/1000 of an inch apart

(b) Using 100 slices 0.02 mm apart

Figure 5: Scatter plots showing the relationship between separation of B-scan slices (horizontal axis) and the estimated separation as a multiple of resolution cell size (vertical axis).

[1]Dynamic Imaging, Cochrane Square, Brucefield Industrial Park, Livingston EH54 9DR, Scotland, UK.

The second experiment involved a tissue-mimicking phantom manufactured by the Department of Medical Physics at the University of Wisconsin, Madison, Wisconsin, USA [4]. This phantom contains a regular planar grid of spheres 2 mm in diameter, that have been carefully designed to have the same speed of sound and attenuation properties as the surrounding material, but no back-scattering material. They therefore appear black in the B-scans but do not introduce other distortions into the image [6].

The phantom was scanned freehand, without a position sensor, using the Diasus ultrasound machine and a 10 MHz rectilinear probe with a 6 cm depth setting. The 3D reconstruction methodology described in section 4 was applied, using a Polaris optical tracker[2] to determine the elevational dimensions of the resolution cell. Figure 6(b) shows a planar reslice calculated at right angles to the original B-scans. The actual horizontal sphere spacing is 15 mm; using the regression algorithm, the measured distance between marker 1 and marker 2 is 14.04 mm, and between marker 2 and marker 3 is 14.72 mm.

To obtain a more detailed measure of the distortion from the image-based reconstruction, an automatic algorithm was used to refine the locations of the sphere centres, and the 3D locations of these centre points were then aligned with a regular grid of the correct dimensions using a non-linear optimisation algorithm (Levenberg-Marquardt [7]). The algorithm for locating the sphere centres involved multiplying each B-scan with a 2D mask, with radius 1 mm, of the form $m(x, y) = (1 - \sqrt{x^2 + y^2}), (0 \leq m \leq 1)$, around the approximate location of each of the spheres. The point of minimum response indicated the centre point of the intersection of the sphere with the B-scan. The 3D location of the sphere centre was then calculated by assuming that the scans were approximately parallel and interpolating between the three B-scans with the minimum responses.

Figure 6(a) shows the errors between the correct positions of the spheres, indicated as circles, and the centres of the spheres as located by the image-based reconstruction, which are shown as + signs. 95% of the sphere centres are located to within ±1.5mm of their correct position in the best-fit grid.

6 *In vivo* experiments

A freehand 3D ultrasound scan of a 16 week foetus *in utero* was acquired both with and without a position sensor as described above in section 4. A Toshiba[3] Powervision 7000 scanner was used with a 3.5 MHz curvilinear probe. A Fastrak[4] magnetic sensor was used to determine the elevational dimensions of the resolution cell. A reslice through the middle of this data, roughly orthogonal to the original scan planes, was calculated using both positions from the sensor (figure 7(a)), and positions from the regression algorithm (figure 7(b)). Both reslices in figure 7 are reproduced to the same scale. The image-based reslice clearly provides a reasonable representation of the object scanned, but there is a

[2]Northern Digital Inc., Randall Drive, Waterloo, Ontario, Canada.

[3]Toshiba Medical Systems Europe, Zilverstraat 1, 2718 RP, Zoetermeer, Netherlands.

[4]Polhemus Inc., 40 Hercules Drive, Colchester, Vermont, Canada

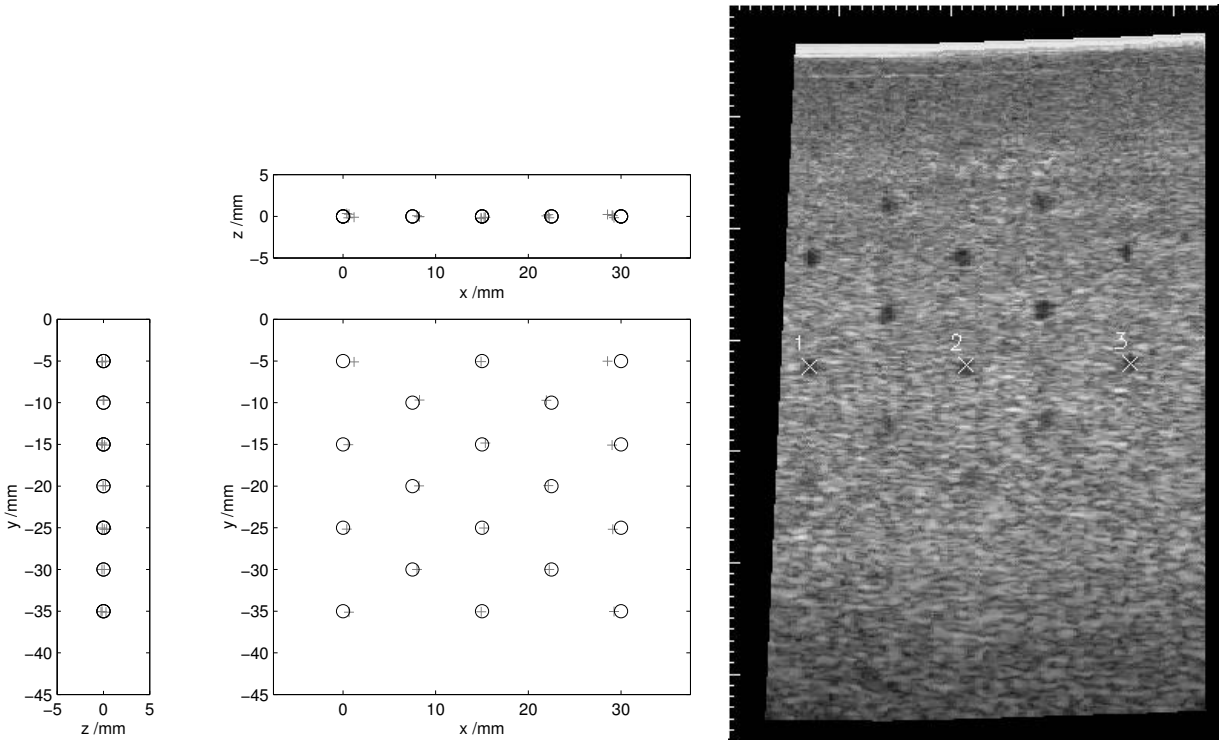

(a) Locations of spheres identified by regression algorithm

(b) Reslice through 3D data of speckle phantom

Figure 6: A freehand scan is taken of a speckle phantom containing a regular grid of spheres with very low scattering properties. In (a) we show the errors of reconstructed sphere centres relative to a best-fit regular grid. (b) is a reslice through the acquired 3D data.

noticeable compression of the image in the longitudinal direction relative to the equivalent sensor-based image.

Figure 8 shows surfaces derived from a scan of a different 16 week foetus where the 3D positions are either provided directly by a position sensor, or calculated using the regression algorithm. A Toshiba Powervision 6000 scanner was used with a curvilinear probe. The Fastrak magnetic sensor was again used to measure the resolution cell. The outline of the foetus was manually segmented in the original B-scan images. Both parts of the figure are based on the same set of segmentation contours in the same B-scans. In figure 8(a) the B-scans, and hence the contours, are located in 3D space using position sensor information. In figure 8(b) the positions of the contours are determined by the image-based regression algorithm as described in section 4. In both cases, a surface is then constructed through the contours using the techniques described in [10].

The volume of the foetus found using the position sensor data is 104 ml. The volume using positions from the regression algorithm is 94 ml. This represents an error of 9%.

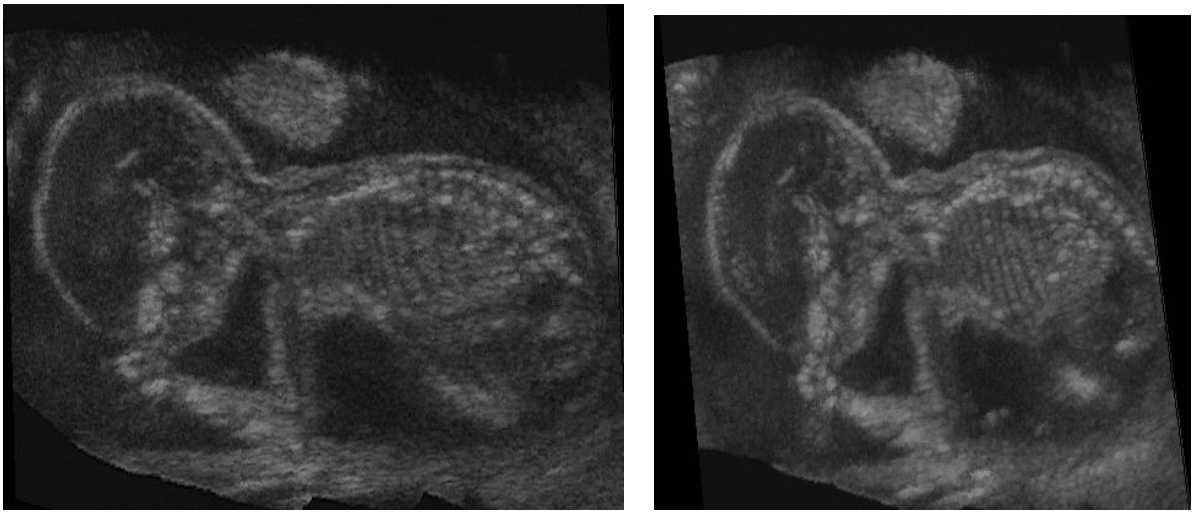

(a) Using a magnetic position sensor

(b) Using regression algorithm

Figure 7: Reconstructed slices through a freehand 3D scan of a 16 week foetus *in utero.*

7 Conclusions

We have presented an analysis of speckle statistics that leads to a new technique for making out-of-plane distance measurements between ultrasound images. Simulation results confirm the theory, and *in vitro* experiments demonstrate that the technique can achieve reasonable accuracy, particularly over short distances. *In vivo* scans show that the technique constitutes a viable approach for visualisation and volume measurement of freehand 3D ultrasound without an external position sensor.

We expect there to be two main applications for this approach; completely sensorless 3D scanning, and use together with a position sensor to improve the short-range accuracy of the acquired data. Because of the inevitable drift associated with a solely image-based approach, it is this second application area that may prove the more important in the long term.

In this report we have confined ourselves to demonstrating the viability of the new regression-based distance measurement algorithm. In appendix A, we show how our theory can be extended to prove the well known correlation-based distance measurement result. It remains to be seen which of the correlation or regression algorithms is best and whether there is a way to make them work together.

8 Acknowledgements

This work was partly supported by grant GR/N21062 from the U.K. Engineering and Physical Sciences Research Council: "High Resolution 3D Ultrasound." Part of figure 1

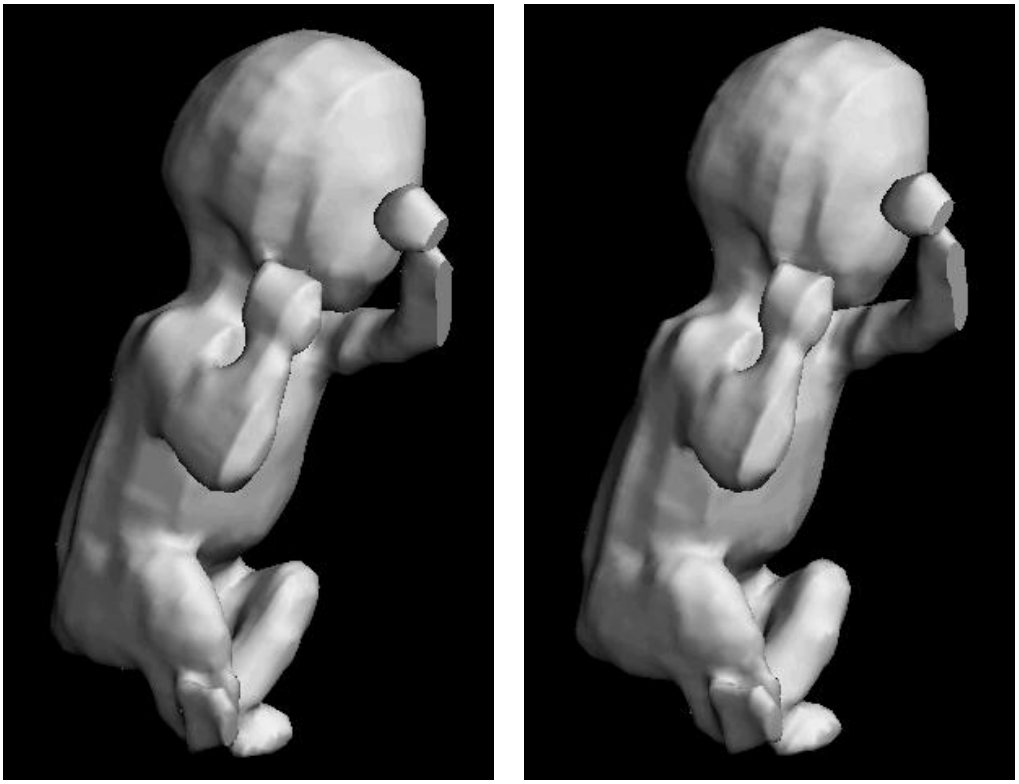

(a) Using magnetic position sensor (b) Using the regression algorithm

Figure 8: Surfaces derived from hand segmentation of a freehand 3D scan of a 16 week foetus *in utero.*

was drawn by Dr Robert Rohling.

A Extension to derive correlation result

We have shown that, for a speckled signal, a linear relationship holds between the intensities of neighbouring resolution cells, while the gradient, b, of this graph tells us how far apart the cells are. This theory can be extended to prove the existing result that the distance between the resolution cells is related to the correlation coefficient, ρ, between the echo intensity values. We need to derive an expression for

$$\rho = \frac{\langle I_1 I_2 \rangle - \langle I_1 \rangle \langle I_2 \rangle}{\sqrt{\langle I_1^2 \rangle - \langle I_1 \rangle^2}\sqrt{\langle I_2^2 \rangle - \langle I_2 \rangle^2}} \tag{15}$$

in terms of the offset, δ, between the resolution cells. We do this by expressing ρ in terms of b, which we know to be related to δ by equation (14).

Both I_1 and I_2 are exponentially distributed so

$$\langle I_1 \rangle = \langle I_2 \rangle = 2\sigma^2 \quad (16)$$

$$\left\langle I_1^2 \right\rangle = \left\langle I_2^2 \right\rangle = 8\sigma^4 \ . \quad (17)$$

The more tricky expression is

$$\begin{aligned} \langle I_1 I_2 \rangle &= \int_0^\infty \langle I_2 | I_1 \rangle \, I_1 \mathrm{p}(I_1) \mathrm{d}I_1 \\ &= \int_0^\infty (bI_1 + a) I_1 \frac{\exp\left(\frac{-I_1}{2\sigma^2}\right)}{2\sigma^2} \mathrm{d}I_1 \\ &= 8b\sigma^4 + 2a\sigma^2 \end{aligned} \quad (18)$$

Substituting equations (16), (17) and (18) into equation (15)

$$\rho = \frac{8b\sigma^4 + 2a\sigma^2 - 4\sigma^4}{2\sigma^2 \times 2\sigma^2} = 2b + \frac{a}{2\sigma^2} - 1$$

Substituting values for b and a from equation (8), and recalling that $2\sigma^2 = \langle I \rangle$:

$$\begin{aligned} \rho &= 2\left(1 - \frac{\langle i \rangle}{\langle I \rangle}\right)^2 + \frac{\langle i \rangle}{\langle I \rangle}\left(2 - \frac{\langle i \rangle}{\langle I \rangle}\right) - 1 \\ &= \left(1 - \frac{\langle i \rangle}{\langle I \rangle}\right)^2 = b \end{aligned} \quad (19)$$

So for an image of fully developed speckle, we expect ρ to be numerically equal to the gradient of our 'best fit' line. Thus ρ varies with distance just as b does.

References

[1] J-F. Chen, J. B. Fowlkes, P. L. Carson, and J. M. Rubin. Determination of scan-plane motion using speckle decorrelation: theoretical considerations and initial test. *International Journal of Imaging Systems Technology*, 8:38–44, 1997.

[2] R. J. Dickinson and C. R. Hill. Measurement of soft tissue motion using correlation between A-scans. *Ultrasound in Medicine and Biology*, 8:263–271, 1982.

[3] M. A. Fischler and R. C. Bolles. Random sample consensus: a paradigm for model fitting with applications to image analysis and automated cartography. *Communications of the ACM*, 24(6):381–395, June 1981.

[4] Jr. J. M. Kofler and E. L. Madsen. Improved method for determining resolution zones in ultrasound phantoms with spherical simulated lesions. *Ultrasound in Medicine and Biology*, 27(12):1667–1676, 2001.

[5] M. Li. System and method for 3D medical imaging using 2D scan data., September 1995. United States patent 5,582,173. Application number 529778.

[6] E. L. Madsen, G. R. Frank, and F. Dong. Liquid or solid ultrasonically tissue-mimicking materials with very low scatter. *Ultrasound in Medicine and Biology*, 24(4):535–542, 1998.

[7] J. J. More. The Levenberg-Marquardt algorithm: implementation and theory. In A. Watson, editor, *Numerical Analysis*, pages 105–116. Lecture Notes in Mathematics 630, Springer-Verlag, 1977.

[8] R. W. Prager, A. H. Gee, G. M. Treece, and L. H. Berman. Speckle detection in ultrasound images using first order statistics. Technical Report CUED/F-INFENG/TR.415, Cambridge University Engineering Department, July 2001.

[9] R. W. Prager, A. H. Gee, G. M. Treece, and L. H. Berman. Decompression and speckle detection for ultrasound images using a homodyned k distribution. *To appear in Pattern Recognition Letters*, 2002.

[10] G. M. Treece, R. W. Prager, A. H. Gee, and L. Berman. Fast surface and volume estimation from non-parallel cross-sections, for freehand 3-D ultrasound. *Medical Image Analysis*, 3(2):141–173, 1999.

[11] G. M. Treece, R. W. Prager, A. H. Gee, and L. H. Berman. Correction of probe pressure artifacts in freehand 3D ultrasound. *To appear in Medical Image Analysis*, 2002.

[12] T. A. Tuthill, J. F. Krücker, J. B. Fowlkes, , and P. L. Carson. Automated three-dimensional US frame positioning computed from elevational speckle decorrelation. *Radiology*, 209:575–582, 1998.

[13] R.F. Wagner, M. F. Insana, and D. G. Brown. Statistical properties of radio-frequency and envelope-detected signals with applications to medical ultrasound. *Journal of the Optical Society of America A*, 4(5):910–922, May 1987.